Monthly Notices
of the
ROYAL ASTRONOMICAL SOCIETY

MNRAS **436,** 3614–3625 (2013)
Advance Access publication 2013 October 23

doi:10.1093/mnras/stt1839

Nebular spectroscopy of the nearby Type IIb supernova 2011dh

Isaac Shivvers,[1]★ Paolo Mazzali,[2,3] Jeffrey M. Silverman,[4]† János Botyánszki,[5] S. Bradley Cenko,[1,6] Alexei V. Filippenko,[1] Daniel Kasen,[1,5,7] Schuyler D. Van Dyk[8] and Kelsey I. Clubb[1]

[1]*Department of Astronomy, University of California, Berkeley, CA 94720-3411, USA*
[2]*Astrophysics Research Institute, Liverpool John Moores University, Liverpool L3 5UZ, UK*
[3]*Max-Planck-Institut für Astrophysik, Karl-Schwarzschildstr. 1, D-85748 Garching, Germany*
[4]*Department of Astronomy, University of Texas, Austin, TX 78712, USA*
[5]*Department of Physics, University of California, Berkeley, CA 94720, USA*
[6]*Astrophysics Science Division, NASA/Goddard Space Flight Center, Mail Code 661, Greenbelt, MD 20771, USA*
[7]*Nuclear Science Division, Lawrence Berkeley National Laboratory, Berkeley, CA 94720, USA*
[8]*Spitzer Science Center/Caltech, Mailcode 220-6, Pasadena, CA 91125*

Accepted 2013 September 26. Received 2013 September 25; in original form 2013 July 3

ABSTRACT

We present nebular spectra of the nearby Type IIb supernova (SN) 2011dh taken between 201 and 678 d after core collapse. At these late times, SN 2011dh exhibits strong emission lines including a broad and persistent Hα feature. New models of the nebular spectra confirm that the progenitor of SN 2011dh was a low-mass giant ($M \approx 13$–$15\,M_\odot$) that ejected $\sim 0.07\,M_\odot$ of ^{56}Ni and $\sim 0.27\,M_\odot$ of oxygen at the time of explosion, consistent with the recent disappearance of a candidate yellow supergiant progenitor. We show that light from the SN location is dominated by the fading SN at very late times (~ 2 yr) and not, for example, by a binary companion or a background source. We present evidence for interaction between the expanding SN blast wave and a circumstellar medium at late times and show that the SN is likely powered by positron deposition $\gtrsim$1 yr after explosion. We also examine the geometry of the ejecta and show that the nebular line profiles of SN 2011dh indicate a roughly spherical explosion with aspherical components or clumps.

Key words: techniques: spectroscopic – supernovae: general – supernovae: individual: SN 2011dh.

1 INTRODUCTION

Type IIb supernovae (SNe IIb; Woosley et al. 1987; Filippenko 1988) are a relatively rare class of core-collapse supernova (SN), constituting only ∼7 per cent of all SNe (Li et al. 2011). Like other SNe II, they show strong hydrogen features in their early time spectra, yet within only a few weeks after core collapse the H fades and the spectra of SNe IIb most closely resemble those of stripped-envelope SNe Ib (for a review of the spectral classification of SNe, see Filippenko 1997). SNe IIb therefore represent a transitional class of core-collapse SNe with only partially stripped envelopes. Exactly what process removes most (but not all) of their hydrogen envelope is still an open question, though interaction with a binary companion increasingly appears to be the most likely answer.

Thus far, there have been only a handful of nearby and intensely studied SNe IIb, including SN 2008ax (∼9.6 Mpc; e.g. Chornock et al. 2011), SN 2001ig (∼11.5 Mpc; e.g. Silverman et al. 2009), SN 2003bg (∼21.7 Mpc; e.g. Hamuy et al. 2009; Mazzali et al. 2009) and SN 1993J (∼3.69 Mpc; e.g. Filippenko, Matheson & Ho 1993; Matheson et al. 2000a). SN 2011dh in M51 (∼8.05 Mpc; see Section 2.3) has become another nearby and very well-observed example of this unusual class of SN.

In early 2011 June, SN 2011dh (also known as PTF11eon) was independently discovered within ∼1 d of core collapse by several amateur astronomers (Griga et al. 2011) and the Palomar Transient Factory (PTF) collaboration (Law et al. 2009; Rau et al. 2009; Arcavi et al. 2011). The SN is apparent in an image taken by A. Riou of France on May 31.893 (UT dates are used throughout), while a PTF image taken on May 31.275 does not detect a source down to a 3σ limiting magnitude of $m_g = 21.44$ (Arcavi et al. 2011). These observations most likely bracket the time of explosion, and for this paper we assume an explosion date of May 31.5. After discovery, a spectrum was promptly obtained by Silverman, Filippenko & Cenko

★ E-mail: ishivvers@astro.berkeley.edu
† NSF Astronomy and Astrophysics Postdoctoral Fellow.

(2011), and a possible progenitor star was first identified in archival *Hubble Space Telescope (HST)* images by Li & Filippenko (2011).

Maund et al. (2011) and Van Dyk et al. (2011) confirmed the identification of the likely progenitor star in *HST* images through ground-based adaptive optics imaging of the SN, measuring a spatial coincidence of the *HST* source and the SN to within 23 and 7 mas, respectively. Both reported that the source in the *HST* images has a spectral energy distribution consistent with a single star: a yellow (mid-F) supergiant with an extended envelope ($R \approx 200\,R_\odot$), a temperature of $\sim$6000 K and a mass of 13–18 $M_\odot$. However, Van Dyk et al. (2011) expressed doubt that the yellow supergiant (YSG) is the true progenitor of SN 2011dh, instead preferring a scenario with a faint and compact progenitor as a binary companion to the YSG. This was largely motivated by the results of Arcavi et al. (2011), who favoured a compact (10^{11} cm) binary companion based on the rapidity of the shock breakout and the relatively cool early photospheric temperature. Soderberg et al. (2012) supported this interpretation with radio and X-ray observations, estimating the progenitor size to be $\sim 10^{11}$ cm through modelling of the cooling envelope. In this compact star scenario, the progenitor of SN 2011dh was theorized to be a faint Wolf–Rayet star with a zero-age main-sequence mass $\gtrsim 25\,M_\odot$ and a history of mass-loss through vigorous winds.

Bersten et al. (2012) disagreed; their hydrodynamical models suggested that an extended progenitor was required to produce the early time light curve, at odds with the analytic relation used by Arcavi et al. (2011), originally from Rabinak & Waxman (2011). Bersten et al. (2012) found that a progenitor with a zero-age main-sequence mass of 12–15 $M_\odot$ and a radius of $\sim 200\,R_\odot$ was consistent with the early time light curve and photospheric temperature, and showed that any model with a zero-age main-sequence mass $\gtrsim 25\,M_\odot$ (i.e. a Wolf–Rayet star) was strongly disfavoured. Benvenuto, Bersten & Nomoto (2012) presented a model of a possible binary progenitor scenario with a $\sim 16\,M_\odot$ YSG primary star losing material to a much fainter $\sim 10\,M_\odot$ companion (undetectable in the pre-explosion *HST* images).

In addition, Murphy et al. (2011) argued that the mass of the SN 2011dh progenitor must be either $13^{+2}_{-1}\,M_\odot$ or $>29\,M_\odot$, based upon an analysis of the star formation history of the SN's environment. Star formation in the vicinity of the SN overwhelmingly occurred in two discrete bursts at <6 and 17^{+3}_{-4} myr; the zero-age main-sequence mass of the SN progenitor is constrained by assuming that the star is associated with one of those events, taking into account errors due, for example, to uncertain late-stage stellar evolution and mass-loss. This result is consistent with the YSG progenitor scenario. Throughout 2012 other authors presented further panchromatic observations, some of which favoured a compact progenitor while others suggested an intermediate or extended progenitor, emphasizing the need for a definitive progenitor identification (e.g. Bietenholz et al. 2012; Campana & Immler 2012; Horesh et al. 2012; Krauss et al. 2012; Sasaki & Ducci 2012).

The desired identification was provided by Van Dyk et al. (2013), who reported that the YSG progenitor candidate had disappeared from new *HST* images. Specifically, at an age of $\sim$641 d SN 2011dh had faded down to 1.30 and 1.39 mag fainter than the YSG progenitor in the *HST* Wide Field Camera 3 *F*555*W* and *F*814*W* passbands, respectively. This result is corroborated by Ergon et al. (2013), who report a significant decline in the *B*-, *V*-, and *r*-band fluxes between pre-explosion imaging of the YSG progenitor and imaging of the SN at 600+d past explosion. These results clearly point towards the extended YSG progenitor found in archival *HST* images as the progenitor star of SN 2011dh.

In this paper, we present six new spectra of SN 2011dh taken between 201 and 678 d after core collapse, in the nebular phase of its evolution. During the nebular phase, the SN ejecta are optically thin and we can directly observe the products of explosive nucleosynthesis without reprocessing through a photosphere. Our very late time spectra show that the flux observed by Van Dyk et al. (2013) and Ergon et al. (2013) was produced primarily by the fading SN and not a stellar source. We present models of the nebular emission spectra and detailed analyses of the line profiles and the late time flux energetics, providing constraints on the progenitor's mass and composition and the geometry of the explosion. We describe our observations and data-reduction procedure in Section 2, present our spectra and analysis in Section 3, discuss our model spectra in Section 4 and conclude in Section 5.

2 OBSERVATIONS AND DATA REDUCTION

2.1 Spectroscopy

Following its discovery in early 2011 June, we began an extensive spectroscopic monitoring campaign of SN 2011dh. Some of our early time spectra from the Lick and Keck Observatories (including a spectrum obtained only 2.4 d after explosion) have already been presented by Arcavi et al. (2011), and other groups have published their own spectra (Ergon et al. 2013; Marion et al. 2013; Sahu, Anupama & Chakradhari 2013). This study focuses on the nebular phase of SN 2011dh.

We collected spectra using both the Lick and Keck Observatories, moving to a larger aperture as the SN faded away. We used the Kast double spectrograph on the Shane 3 m telescope at Lick Observatory (Miller & Stone 1993), the Low Resolution Imaging Spectrometer (LRIS) mounted on the 10 m Keck I telescope (Oke et al. 1995) and the DEep Imaging Multi-Object Spectrograph (DEIMOS) on the 10 m Keck II telescope (Faber et al. 2003) to collect 3, 1 and 2 nebular spectra of SN 2011dh, respectively. Table 1 summarizes observing details for these six spectra.

2.2 Data reduction

All observations were collected and reduced following standard techniques as described by Silverman et al. (2012). All spectra were taken with the slit oriented at the parallactic angle to minimize flux losses caused by atmospheric dispersion (Filippenko 1982). We use a low-order polynomial fit to arc-lamp observations to calibrate the wavelength scale, and we flux calibrate each spectrum with a spline fit to standard star spectra observed on the same night at a similar air mass. In addition, we have removed telluric absorption lines from all spectra. Upon publication, all raw spectra presented in this paper will be made available in electronic format on the Weizmann Interactive Supernova data REPository (WISeREP; Yaron & Gal-Yam 2012).[1]

2.3 Distance

The distance to M51 has been measured through several independent methods with significant scatter among their results. We follow Marion et al. (2013) and adopt $D = 8.05 \pm 0.35$ mpc, an average of four of these measures (Tully & Fisher 1988; Feldmeier, Ciardullo

[1] http://www.weizmann.ac.il/astrophysics/wiserep

Table 1. Journal of spectroscopic observations.

UT date	Day[a]	Instrument	Range (Å)	Resolution (Å)[b]	Exposure time (s)
2011 December 18	201	Kast	3480–10114	7	2400
2011 December 24	207	Kast	3428–10100	6	2100
2012 February 23	268	Kast	3444–10166	6	3000
2012 April 29	334	LRIS	3312–7360	3	600
2013 February 17	628	DEIMOS	4500–9640	3	2400
2013 April 8	678	DEIMOS	4450–9603	3	3600

[a]Days since explosion (2011 May 31.5).
[b]Approximate resolution (averaged over spectrum).

& Jacoby 1997; Tonry et al. 2001; Vinkó et al. 2012). All spectra have been deredshifted by M51's recession velocity, 600 km s^{-1} ($z = 0.002$, NED; Rush, Malkan & Edelson 1996). M51 is at very low redshift and so we neglect time-dilation effects due to cosmological expansion. Both Arcavi et al. (2011) and Vinkó et al. (2012) use high-resolution spectra to measure the reddening towards M51 using Na I D absorption-line widths. Both find the host galaxy extinction to be negligible and the Milky Way extinction to be consistent with values measured by Schlegel, Finkbeiner & Davis (1998): $E(B-V) = 0.035$ mag. We deredden all spectra by this value prior to analysis, using the reddening law of Cardelli, Clayton & Mathis (1989) and assuming $R_V = 3.1$. Note that Ergon et al. (2013) adopted a slightly higher value of $E(B-V) = 0.07^{+0.07}_{-0.04}$ mag, corresponding to a ∼5–10 per cent difference in absolute flux level across the optical spectrum, not enough to significantly affect the discussion below.

2.4 Absolute flux calibration

Our observation techniques and data-reduction methods record the relative flux with high fidelity, but absolute flux calibrations are a persistent difficulty in long-slit spectroscopy. Variations in atmospheric seeing between flux-standard observations and science observations can result in varying amounts of flux falling out of the slit and spectral observations are often taken in less-than-photometric conditions with non-negligible (and possibly varying) levels of cloud cover. Parts of our analysis (see Sections 3.1 and 4) require an absolute flux measure, however, so we address this problem by flux calibrating our spectra to late time photometry of SN 2011dh wherever possible.

Tsvetkov et al. (2012) present *UBVRI* light curves of SN 2011dh extending to just over 300 d; we assume a linear decay in *R*-band magnitudes beyond ∼70 d and perform a maximum-likelihood analysis to estimate the *R* magnitude of SN 2011dh at the time each spectrum was taken. We chose the *R* band because of its relatively dense coverage and because several of the strongest nebular lines ([O I], [Ca II], Na I, Hα) fall within the passband, making it a good tracer of the SN's decline. We match synthetic photometry of our 201–334 d spectra to these values. All synthetic photometry has been calculated with `pysynphot` (Laidler et al. 2008). As shown in Fig. 1, we find an *R*-band decline rate of 0.0195 ± 0.0006 mag d^{-1} and a *V*-band decline rate of 0.0207 ± 0.0009 mag d^{-1} (reported errors are 68 per cent confidence levels; $\sim 1\sigma$).

A linear decay in magnitudes is a reasonable assumption so long as emission is primarily driven by the radioactive decay of ^{56}Co (e.g. Colgate & McKee 1969; Arnett 1996). It is common for SNe Ib/IIb to display decline rates significantly faster than the $^{56}\mathrm{Co} \rightarrow {}^{56}\mathrm{Fe}$ rate (0.0098 mag d^{-1}) – a steep decline rate is reasonably interpreted as evidence for a declining γ-ray trapping fraction in the ejecta (as the ejecta expand and the density drops, more of the γ-rays produced by ^{56}Co decay escape before depositing their energy). The decline rate of SN 2011dh is slightly faster than those measured for both SN 1993J and SN 2008ax, two well-understood SNe IIb which had decline rates of 0.0157 and 0.0164 mag d^{-1}, respectively (fit to days ∼60–300; Taubenberger et al. 2011). See Section 3.1 for a comparison between these early time nebular decline rates and the flux observed at very late times (>600 days).

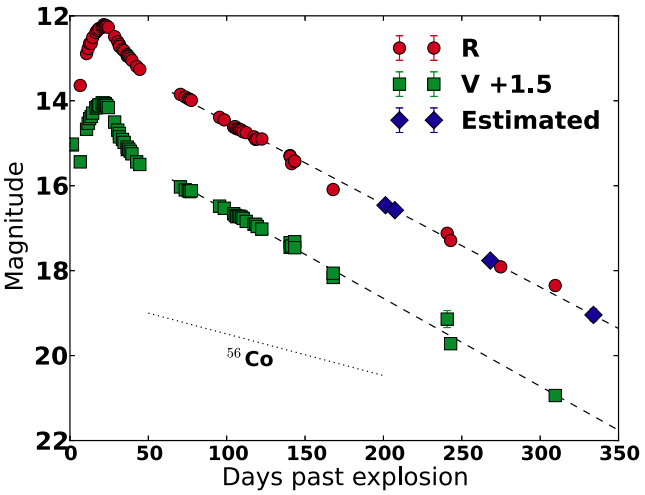

Figure 1. Photometric decline of SN 2011dh from Tsvetkov et al. (2012), with our best-fitting decline rates and the ^{56}Co decay rate overplotted. The blue (diamond) points are the estimated values used to flux calibrate our spectra between days 201 and 334. Note that error bars for most points are smaller than the plotted symbol.

We do not assume that the same decay law holds true out to our last two spectra, at 628 and 678 d after core collapse. Instead, we repeat the analysis described above using photometry from Ergon et al. (2013), who report Nordic Optical Telescope (NOT) observations in *V* at 601 and 685 d.

3 ANALYSIS

By 201 d past explosion SN 2011dh was well into the nebular phase, with a spectrum dominated by strong emission lines and little or no continuum. Fig. 2 shows our complete spectral sequence of SN 2011dh in the nebular phase with spectra from 201 to 678 d after explosion and a few prominent lines identified, and compares the spectra of SN 2011dh to those of a few other prominent SNe IIb at comparable epochs.

Throughout the first year after explosion the nebular spectra of SN 2011dh are dominated by strong [O I] λλ6300, 6364 and

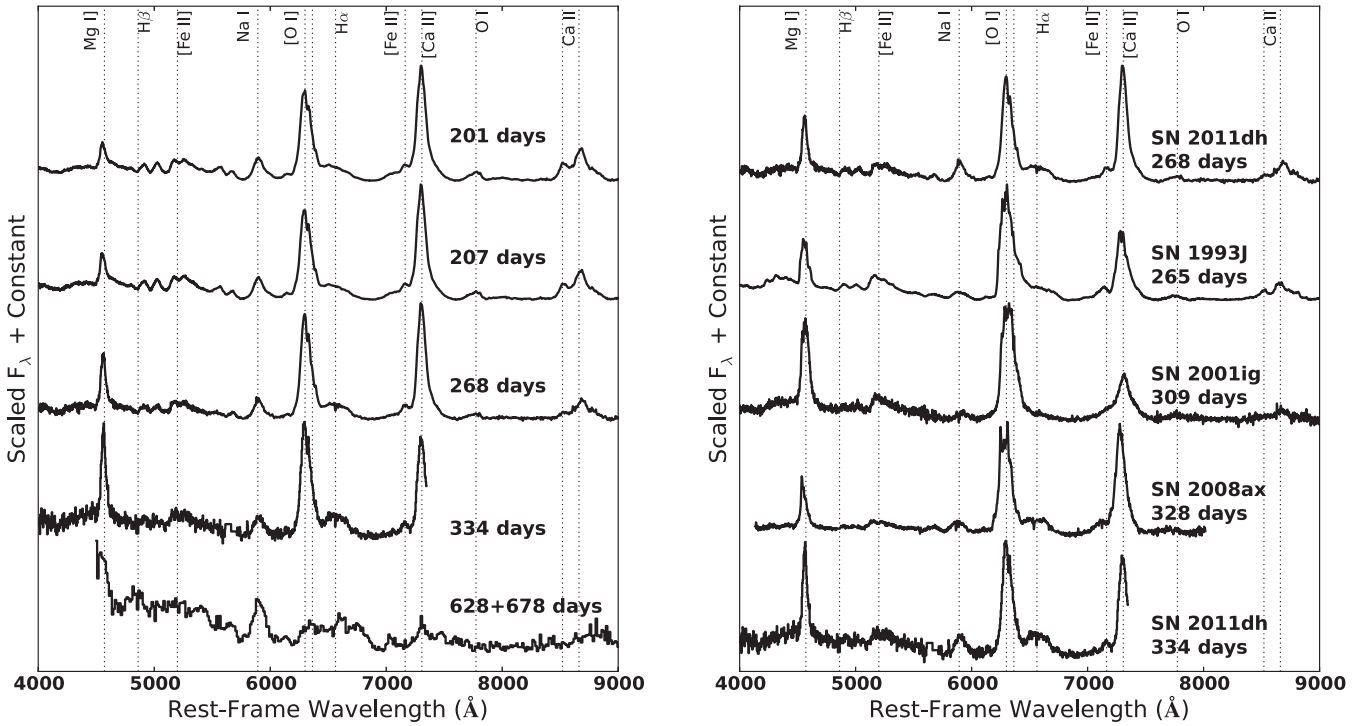

Figure 2. Nebular spectra of SN 2011dh (left) and comparison spectra of SN 1993J, SN 2001ig and SN 2008ax (right). All spectra have been deredshifted. All displayed SNe are at low redshift and time-dilation effects are negligible; listed phases are days since explosion in Earth's reference frame. The spectra of SN 2011dh from 628 and 678 d have been co-added and rebinned to increase the signal-to-noise ratio (S/N). The SN 1993J spectrum is from Filippenko, Matheson & Barth (1994) and Matheson et al. (2000b), the SN 2001ig spectrum is from Silverman et al. (2009) and the SN 2008ax spectrum is from Milisavljevic et al. (2010).

Table 2. Integrated line fluxes relative to [Ca II] λλ7291, 7324.

Day[a]	[Ca II] + Fe II[b]	Mg I]	Na I D	Ca II[c]	O I λ7774	Hα[d]	[O I] λλ6300, 6364[e]
201	1.0	0.114	0.151	0.403	0.059	0.196	0.614
207	1.0	0.140	0.147	0.369	0.059	0.222	0.621
268	1.0	0.218	0.135	0.247	0.039	0.253	0.749

Notes. Errors are difficult to estimate for these values, as line edges and continuum levels have been estimated by eye. However, care was taken to treat each line similarly. Measurement errors alone (determined through repeated measurements) are ∼5 per cent.

[a]Days since explosion (2011 May 31.5).

[b][Ca II] λλ7291, 7324 and Fe II λ7155 are difficult to deblend, so we present the integrated flux of both. The contribution from Fe II is, however, very much smaller than [Ca II] (see Fig. 2).

[c]The Ca II near-infrared triplet.

[d]To measure the blended [O I] and Hα lines we assume Hα is symmetric about the rest wavelength (6563 Å). We report the Hα flux as twice the value obtained by integrating from the red continuum to 6563 Å.

[e]The [O I] line was integrated after subtracting a smoothed Hα profile, again assuming symmetry about 6563 Å in the Hα line.

[Ca II] λλ7291, 7324 emission lines, alongside a strong Mg I] λ4571 emission line and persistent Na I D and Hα lines. Table 2 lists relative line strengths of several prominent lines in the early nebular phase. We measured these fluxes by subtracting a local linear continuum and integrating over each line. Note that the continuum here is not from the photosphere of the SN, but rather is likely a mixture of blended lines, producing a sort of pseudo-continuum. Also, note that this type of integrated flux measurement is by no means exact due to line blending and the approximated local continuum, but care was taken to treat each line similarly and these measures should accurately portray the relative-flux trends.

The relative flux of [Ca II] and [O I] has been shown to be a useful indicator of progenitor core mass, with smaller [O I]/[Ca II] ratios generally indicative of a less massive helium core at the time of explosion (e.g. Fransson & Chevalier 1989; Jerkstrand et al. 2012). SN 2011dh displays an [O I]/[Ca II] ratio significantly smaller than that in both SN 1993J and SN 2001ig. The ratio is similar to that in SN 2008ax, which also displayed a similar upward trend throughout the nebular phase (Filippenko et al. 1994; Silverman et al. 2009; Chornock et al. 2011). It therefore appears that SN 2011dh's progenitor He core mass was relatively close to that of SN 2008ax and significantly less than that of both

SN 2001ig and SN 1993J. See Section 4 for a more thorough analysis.

There appears to be a weak blue continuum in the 600+d spectra of SN 2011dh. Maund et al. (2004), in a very high S/N spectrum of SN 1993J taken ∼10 yr after explosion, were able to associate a blue continuum (and a detection of the Balmer absorption-line series) with a companion B supergiant, thereby strongly supporting the binary nature of the SN and identifying the components – a K-giant progenitor and a B-giant companion. In the spectrum of SN 2011dh above, however, we cannot attribute the blue continuum to any stellar companion: fitting a Rayleigh–Jeans curve to the apparent continuum yields best-fitting temperatures much too hot for a stellar source. The blue continuum in SN 2011dh is instead most likely a pseudo-continuum caused by many blended lines. In addition, our spectra are more noisy at the blue end, and the blue rise may be partially caused by increased noise. *HST* photometry taken near this time provides a slightly redder colour than synthetic photometry from our spectrum: $F555W - F814W = 0.69 \pm 0.03$ mag (641 d; Van Dyk et al. 2013), compared to ∼0.34 mag from our spectrum (628+678 d). Thus, we tilt our spectrum to match the *HST* $F555W - F814W$ colour and re-examine the result for evidence of a stellar companion. Our conclusion is essentially unchanged: even after tilting our spectrum, the blue pseudo-continuum yields unreasonably hot best-fitting blackbody temperatures.

Interestingly, there is a broad Hα emission line in spectra of SN 2011dh through at least 334 d, similar to the emission seen in SN 1993J, (Filippenko et al. 1994), SN 2007Y (Stritzinger et al. 2009) and SN 2008ax (Milisavljevic et al. 2010) around the same time. There is also some indication of very broad Hα in the spectra of SN 2011dh at 600+d, though the S/N is low. At late times the Hα emission of SN 1993J was unambiguously identified with interactions between the expanding SN shock wave and circumstellar material produced by mass-loss from the progenitor (e.g. Patat, Chugai & Mazzali 1995; Houck & Fransson 1996; Matheson et al. 2000b). As we discuss in Section 3.1, SN 2011dh seems to present us with a more complex situation.

SN 2011dh, like SN 2001ig, displayed a relatively strong Mg I] λ4571 line – significantly more prominent than Mg I] in spectra of SN 2008ax (Silverman et al. 2009; Chornock et al. 2011). This is especially apparent around day 334, where Mg I] emission almost matches the emission in [Ca II] and [O I]. At very late times, in the 628+678 d spectrum, the Mg I] is still quite apparent, though [O I] and [Ca II] have faded into the noise. Unfortunately, our 628 and 678 d spectra do not go much blueward of the Mg I] emission peak; this, together with high noise levels at the blue end, prevents us from measuring the integrated flux reliably at these times. The Na I D flux is also remarkably strong in the 600+d spectra, as discussed below.

3.1 The spectrum of SN 2011dh at 600+d

Recent photometry of the site of SN 2011dh taken by *HST* (Van Dyk et al. 2013) and the NOT (Ergon et al. 2013) provide late time flux measurements of SN 2011dh. Our latest two spectra, taken around the same time, confirm that the optical flux measured by these groups was predominantly from the SN remnant and not, for example, from a binary companion to the progenitor star. 678 d after explosion, SN 2011dh continues to show clear Na I D emission with approximately the same width as at earlier epochs (see Fig. 3). [Ca II] emission is present but much reduced relative to Na I D, Mg I] is still relatively strong but is buried in the noise at the blue end of the spectrum, and there is a very broad feature near 6500 Å – most likely a blend of broad Hα and the [O I] doublet.

Ergon et al. (2013) report a slight fading of 2011dh between days 601 and 685: 0.009 ± 0.0026 mag d^{-1} in V. The V-band decline rate between the last observation reported by Tsvetkov et al. (2012, 19.44 ± 0.12 mag, 2012 April 4, 310 d) and the first observation by

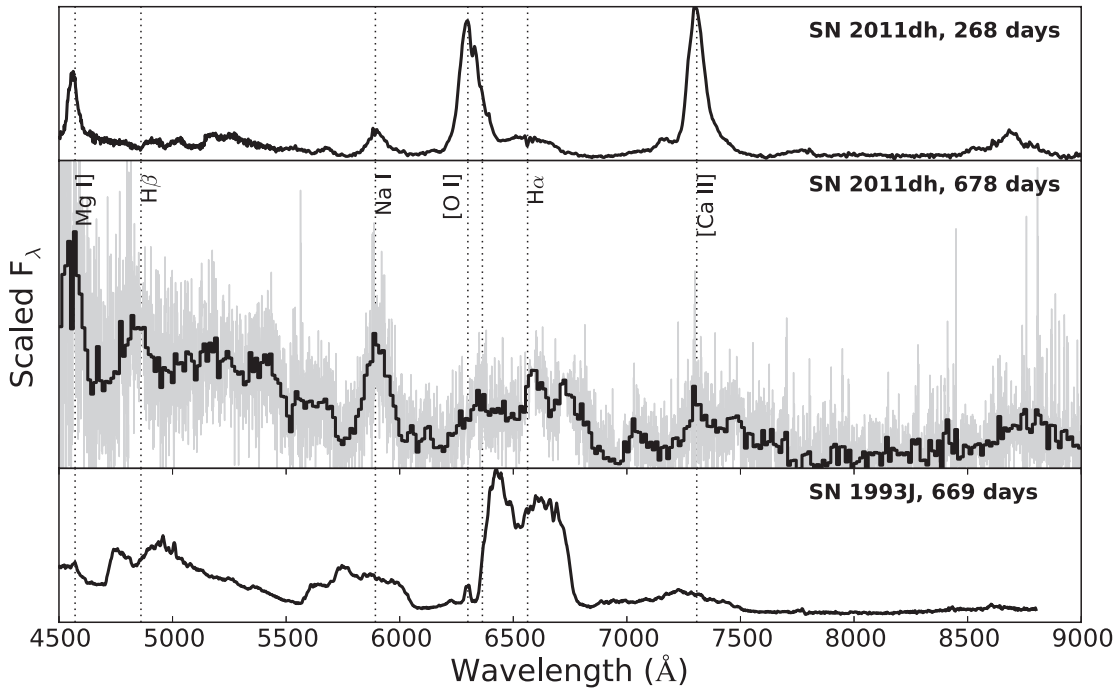

Figure 3. SN 2011dh at 268 and 678 d, with SN 1993J at a similar epoch for comparison (SN 1993J spectrum from Matheson et al. 2000b). The later spectrum of SN 2011dh has been rebinned to increase the S/N; the unbinned spectrum is shown in the background. In both SNe, the broad Hα emission likely comes from interaction between an expanding shockwave and the circumstellar medium, but the Na I D line emission in SN 2011dh is most likely powered by ^{56}Co decay while SN 1993J has a Na I D line powered by CSI.

Table 3. Photometric normalizations.

Day[a]	Passband	Mag $\pm 1\sigma$	Na I D flux[b]
201	*R*	16.46 ± 0.06	36.26 ± 2.10
207	*R*	16.58 ± 0.07	31.95 ± 2.24
268	*R*	17.76 ± 0.10	9.69 ± 1.14
334	*R*	19.04 ± 0.14	4.22 ± 2.45
628	*V*	22.80 ± 0.26	0.338 ± 0.171
628+678[c]	*F555W*	23.198 ± 0.019	0.315 ± 0.098
628+678[c]	*F814W*	22.507 ± 0.022	0.439 ± 0.137
678	*V*	23.32 ± 0.38	0.368 ± 0.243

Notes. Photometric normalizations applied to our nebular spectra and resultant absolute flux in the Na I D line. See Section 2.4 for a description of how we calculated the photometric estimates. We measured the integrated line flux in the manner described in Section 3, and the quoted errors include photometric normalization errors, spectral noise and estimated measurement errors added in quadrature.

[a]Days since explosion (2011 May 31.5).

[b]Units: 10^{-15} erg s^{-1} cm^{-2}.

[c]To estimate the spectrum near the *HST* observations, we produce an average of the 628 and 678 d spectra. We flux calibrate both spectra to $R = 0.0$ mag, co-add them and renormalize the result to the *HST* photometry. This produces an equally weighted average between the two spectra – we assume the SN is changing slowly at this epoch and that this averaged spectrum is a good measure of the relative flux near the average time (653 d).

Ergon et al. (2013, 22.56 ± 0.10 mag, 2013 January 20, 601 days) is ∼0.011 mag d^{-1}. Both of these rates are notably less rapid than the 0.021 mag d^{-1} decline rate measured from the 65–310 d photometry by Tsvetkov et al. (2012, see Section 2.4); it seems that the flux decline rate is slowing down at $t \gtrsim 300$ d.

Na I D provides the clearest feature in our 600+d spectra and is unambiguously associated with the SN (see Fig. 3). We measured the integrated flux in the Na I D line for each of our spectra in the nebular phase; the results are shown in Table 3 and Fig. 4. Note that the absolute flux calibrations of long-slit spectra are often unreliable. As described in Section 2.4, we address this by flux calibrating our spectra to published photometry. Quoted uncertainties include estimated error due to spectral noise, reported photometric errors and estimated measurement errors, all added in quadrature. As Fig. 4 illustrates, the Na I D line flux mirrors the trends in the photometry, falling at the early *R*-band decline rate through ∼300 d but then deviating significantly around 300 or 350 d and fading much more slowly through ∼600 d.

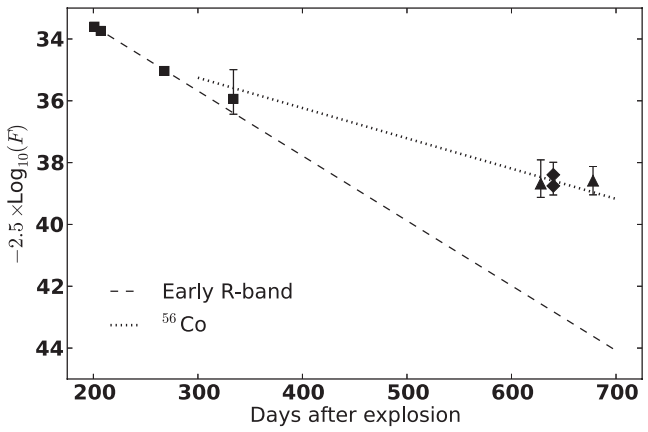

Figure 4. Integrated Na I D flux in nebular spectra of SN 2011dh. All values plotted here are presented in Table 3. The dashed line shows the early time decline rate for the *R* band (see Section 2.4) and the dotted line shows the decline rate of ^{56}Co (0.0098 mag d^{-1}). Boxes are used for spectra normalized to Tsvetkov et al. (2012) photometry, triangles for spectra normalized to Ergon et al. (2013) photometry and diamonds for spectra normalized to Van Dyk et al. (2013) photometry. The positron-dominated epoch appears to begin somewhere between 300–350 d.

This slowdown in the flux decay rate is possibly indicating a transition to γ-ray transparency in the ejecta of SN 2011dh. As described in more detail by Arnett (1996), ^{56}Co radioactivity ($^{56}\mathrm{Co} \rightarrow {}^{56}\mathrm{Fe}$ with a half-life of ∼77 d) is the dominant source of energy for SNe at these epochs. ^{56}Co decay produces both γ-rays and high-energy positrons. The kinetic energy of the positrons is very likely to be deposited into the ejecta (and therefore contribute to the nebular line flux), while the fraction of γ-ray energy that gets deposited depends upon the optical depth of the ejecta to γ-rays. As the ejecta expand and the optical depth drops, a larger fraction of the γ-rays escape, carrying their energy with them.

As the γ-ray energy deposition fraction drops, the SN fades away faster than the ^{56}Co rate (0.0098 mag d^{-1}), until such time as the ejecta are transparent to γ-rays and approximately all of them escape. At that point, positron energy deposition dominates the energy input of the ejecta and the bolometric flux decline rate is expected to follow the ^{56}Co rate closely. Broad-band photometry should exhibit roughly the same behaviour. Assuming that the ejecta's abundance of neutral sodium is constant and that the exposure to heating does not change significantly, so should the Na I D line flux. The flux decline rates for both the late time *V*-band photometry and the Na I D line flux in SN 2011dh are consistent with a transition to a positron-powered ejecta sometime between 300 and 350 d. Because positrons deposit their energy locally (near the decaying ^{56}Co) but γ-rays deposit energy throughout the ejecta, the transition to a positron-dominated energy input is likely to correspond to a change in the dominant emission lines. In SN 2011dh, we see that Na I D and Mg I] emission stays strong in the positron-dominated epoch while [O I] and [Ca II] fade away. More detailed modelling is necessary to test this scenario, however.

Note that the above discussion assumes the bolometric light curve is completely powered by ^{56}Co. Any additional energy input could be a confounding factor; most importantly, there may be a flux contribution from shockwave interactions with circumstellar gas. The progenitors of SNe IIb are stars that have lost much of their hydrogen envelope, either through radiative winds or through stripping by a binary companion. If a significant amount of that material remains nearby in a cloud of circumstellar matter, the expanding SN ejecta will impact it and form a shock boundary. This shocked region produces high-energy photons which are then reprocessed down to optical wavelengths by material in the outer shells of the ejecta, thereby producing broad emission lines and (possibly) a blue pseudo-continuum (for a more complete description of this process, see, e.g. Fransson 1984; Chevalier & Fransson 1994). Late time emission from circumstellar interaction (CSI) is common in SNe IIn (e.g. Fox et al. 2013), which have lost a majority of their envelope in the years prior to explosion, and it has been observed in other SNe IIb (e.g. Matheson et al. 2000b).

CSI could be augmenting the Na I D flux discussed above through either Na I D or He I λ5876 emission. As Fig. 3 shows, SN 1993J clearly displayed a shockwave-powered Na I D + He I blend with ∼1/3 the flux of the Hα line (Matheson et al. 2000b). In the Chevalier & Fransson (1994) model, approximately all of the shockwave-powered Na I D flux is emitted from a thin shell at the boundary between the unshocked circumstellar material and the

shocked ejecta, while the Hα flux comes from both the thin shell and the shocked ejecta. This would imply a more boxy line profile for Na I D than Hα (see below for further discussion of the nebular Hα line in SN 2011dh). However, the late time Na I D emission of SN 2011dh has a relatively narrow profile with no evidence of the box-like shape that would be expected if it were mostly CSI powered, and the profile does not appear to change significantly between the spectra taken at <1 yr and those taken at >1 yr. It seems clear that, at 600+d, the dominant source of Na I D flux remains radioactive decay and not CSI, though there may well be some small amount of shockwave-powered He I and Na I D emission buried in the noise. If SN 2011dh's CSI-powered Na I D + He I flux were a factor of 3 less than the Hα flux (as was the case in SN 1993J), we would not expect to be able to distinguish it from the noise in our spectra.

Note that the *V*-band data may, in addition, include flux contributions from a CSI-powered blue pseudo-continuum at these late times – the 600+d spectra do indicate a faint continuum blueward of 6000 Å. Because of the large time gap between our spectra at 334 and 628 d, we do not know exactly when this blue pseudo-continuum emerged. It does not seem to evolve significantly between our spectra taken at 628 and 678 d, and so we believe that the flux decline measured around this time by Ergon et al. (2013) (0.009 ± 0.0026 mag d^{-1}) is dominated by the fading ^{56}Co contribution and not by any evolving CSI-powered flux. Note that *V*-band photometry likely also includes contributions from the Na I D, [O I], [Fe II] and Hα lines, whether they are powered by radioactivity or CSI – a rather complex puzzle to decode. However, this complexity does not affect the measurement of individual line fluxes. As described above, the Na I D line indicates that the ejecta of SN 2011dh became fully γ-ray transparent (and therefore powered through positron energy deposition) between 300 and 350 d after core collapse.

In contrast with the Na I D line, the nebular Hα line appears to be fuelled entirely through CSI. Assuming the broad feature near 6563 Å in the 678 d spectrum of SN 2011dh (see Fig. 3) is a broad and boxy Hα feature, it exhibits a full width at half-maximum intensity of roughly 21 000–26 000 km s^{-1} (there are large errors when measuring the line width, as this spectrum has a low S/N and the line is weak). Spectra taken in the first month after core collapse show a blueshifted Hα absorption component around 15 400 to 12 500 km s^{-1} (velocities at 4 to 14 d; Marion et al. 2013). These measurements mesh with the CSI scenario described above, wherein the unslowed outer ejecta impact the circumstellar material and produce a shell of emitting gas that continues to move outward at its initial expansion velocity.

The scenario that SN 2011dh presents to us in its late-stage evolution is notably different than that of SN 1993J or SN 1987A. As shown by Suntzeff et al. (1992), the peculiar Type II-P SN 1987A exhibited a continuously declining (yet non-zero) γ-ray opacity until the slowly decaying isotope ^{57}Co became the dominant source of energy around 800–900 d after explosion (^{57}Co $\rightarrow$ ^{57}Fe with a half-life of $\sim$272 d). This indicates that SN 1987A had a significantly higher γ-ray opacity than SN 2011dh. In contrast, CSI became the dominant flux source in SN 1993J around 350 d, when the spectrum became dominated by broad and boxy emission lines (Matheson et al. 2000b), and it is impossible to tell when (or if) the radioactive energy deposition entered the ^{56}Co positron-powered phase. Of course, several questions remain about SN 2011dh and its late time evolution. Unless it rebrightens, however, the SN is too faint to hope for a significantly higher S/N spectrum than those presented here (our spectrum at 678 d represents an hour of integration time on a clear night with the 10 m Keck II telescope). Continued photometric monitoring should provide more information as the SN evolves.

3.2 The oxygen line profile and the ejecta geometry

Fransson & Chevalier (1989) showed that, given the reasonable assumptions of homologous expansion and optically thin emission, the profiles of forbidden lines in nebular SN spectra can be used as tracers of the geometry and density profile of the emitting material. The [O I] $\lambda\lambda$6300, 6364 doublet, specifically, has been used as a diagnostic of ejecta asphericity in SNe Ibc/IIb by many studies (e.g. Mazzali et al. 2005; Maeda et al. 2008; Modjaz et al. 2008; Taubenberger et al. 2009; Maurer et al. 2010; Milisavljevic et al. 2010). The [O I] doublet is generally used because it is consistently one of the strongest lines in nebular SN spectra and is largely isolated and unblended, and oxygen is one of the most abundant elements in stripped-envelope core-collapse SNe. The structure apparent in the [O I] doublet has often been attributed to either a jet or torus geometry in the ejecta with the diversity of line profiles explained through viewing angle dependences (e.g. Mazzali et al. 2005; Maeda et al. 2008; Modjaz et al. 2008), though other explanations have been presented for some SNe (e.g. Maurer et al. 2010; Milisavljevic et al. 2010).

The [O I] profile of SN 2011dh prominently displays multiple peaks and troughs. We explore the geometrical implications of this line profile in two ways. Several studies have previously explored [O I] line profiles by decomposing the profile into a set of overlapping Gaussian curves, effectively assuming a multicomponent Gaussian spatial distribution (e.g. Taubenberger et al. 2009). We performed a similar fit for comparison, but the spatial distribution of emissivity is not necessarily Gaussian; the choice to decompose the profile this way is mainly for convenience. We also ran 3D nebular radiative transfer models for a variety of geometries, attempting to fit the observed line profile with a simple and physically plausible ejecta geometry. [O I] $\lambda\lambda$6300, 6364 is a doublet with two peaks separated by 64 Å, with their relative intensities determined by the local density of neutral oxygen. The intensity ratio reliably approaches 3:1 in nebular SN spectra (e.g. Chugai 1992; Li & McCray 1992), and we assume this holds true for SN 2011dh at these epochs. Before analysing the [O I] profile we remove the Hα emission by assuming that it is symmetric about the rest wavelength (6563 Å) and subtracting a smoothed profile. Note that this nebular spectral analysis is not a well-posed inverse problem; many different geometries could produce the same spectral profile.

The results of our Gaussian decomposition of the line profile are shown in the left-hand panel of Fig. 5. For each component in our fit we specify the amplitude, position and width of the 6300 Å line; the properties of the 6364 Å line are then forced. In the spectrum at 268 d past core collapse, our best fit to the [O I] line requires three such components. There is a broad component blueshifted by $\sim$250 km s^{-1}, a narrow component blueshifted by $\sim$400 km s^{-1} and a second narrow component redshifted by $\sim$1600 km s^{-1}. Note, however, that the broad component is only needed because the overall line profile is distinctly non-Gaussian. A more nuanced approach (below) provides a good fit to the profile with only two components.

The results of our 3D modelling analysis are shown in the right-hand panel of Fig. 5. In our models, we specify the emissivity of the [O I] doublet in each spatial zone and integrate the transfer equation using the Sobolev approximation under the assumption that the ejecta are optically thin (see e.g. Jeffery & Branch 1990). We decompose the 3D emission into multiple overlapping

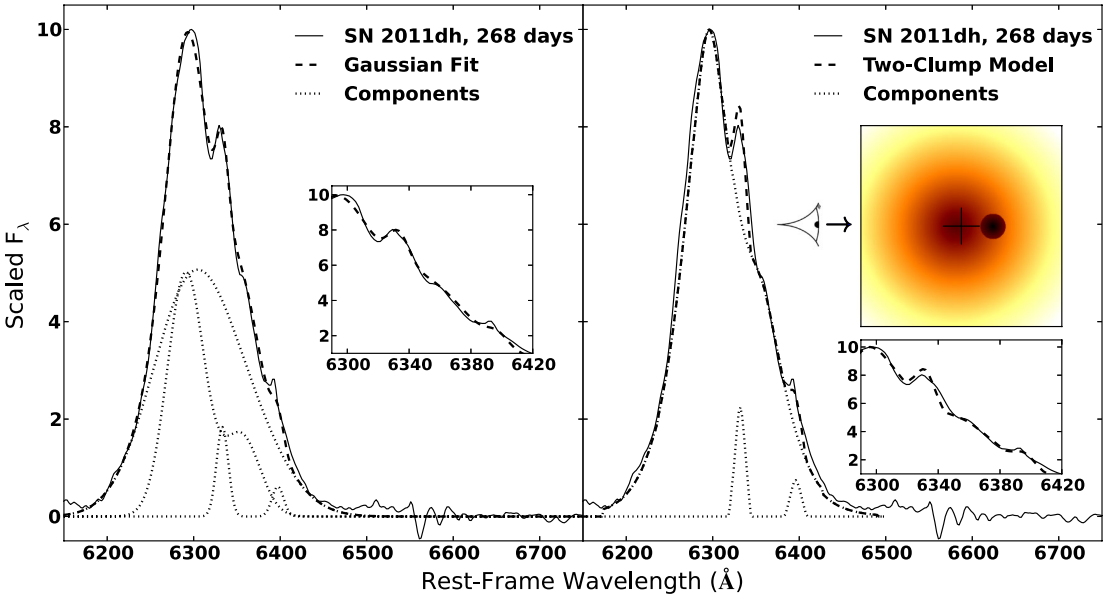

Figure 5. The left-hand panel shows a multi-Gaussian decomposition of SN 2011dh's [O I] λλ6300, 6364 doublet 268 d after explosion. Each component is a doublet with a flux ratio of 3:1 and a wavelength separation of 64 Å. Our best fit includes three such components: a broad central component, a large blueshifted clump and a small redshifted clump. The inset shows a magnified view of the profile's red side. The right-hand panel shows the same observed line profile with our best-fitting two-component model overlaid. The box on the upper right shows a cross-cut through the emissivity profile in velocity space, where the colour gradient represents $\log_{10}$ of emissivity density and the cross marks the rest velocity of M51. The box on the lower right is a magnified view of the right-hand side of the line profile. See Section 3.2 for a complete description.

spherical clumps, each with an exponentially declining emissivity profile. The primary peak is well fitted by a sphere with an emissivity profile characterized by an exponential falloff with *e*-folding velocity $v_e = 950\,\mathrm{km\,s^{-1}}$. To match the position of the peak, we need to offset the entire sphere from the origin towards the observer by $\sim$250 km s^{-1}. The secondary peak is well fitted by placing a second smaller spherical clump along the observer's line of sight but moving away at $\sim$1500 km s^{-1}. The emissivity profile of this second clump has an *e*-folding velocity of $v_e = 300\,\mathrm{km\,s^{-1}}$ which terminates at 600 km s^{-1}. The integrated emission from the primary sphere is $\sim$24 times greater than the integrated emission of the smaller clump, though the peak local emissivity of the smaller clump is a factor of $\sim$4 higher than that of the primary sphere.

The right-hand panel of Fig. 5 shows that this model does a decent job of fitting all features in the [O I] profile. Though this simple model invokes only two components, the true ejecta geometry could in fact consist of multiple clumps of similar or smaller spatial dimensions. This is because it is only the larger inhomogeneities located along the line of sight that produces noticeable and well-separated features in the line profile.

It is unclear whether the clump-like structures we infer from the [O I] doublet correspond to inhomogeneities in the distribution of the oxygen itself or the ^{56}Ni that excites it. In 3D core-collapse simulations, convective motions during neutrino heating act as seeds for Rayleigh–Taylor instabilities that develop when the shock passes through compositional interfaces (e.g. Hammer, Janka & Müller 2010). This results in fingers of heavier elements, such as ^{56}Ni, punching out into the overlying layers of lighter elements. Such a picture could explain the irregular line profiles seen in several core-collapse SNe at late times (e.g. Filippenko & Sargent 1989; Matheson et al. 2000b), and has been explicitly considered previously for the asymmetry seen in SN 1987A. In particular, the substructure noted in the Hα line profile of SN 1987A (the 'Bochum event'; Hanuschik, Thimm & Dachs 1988) has been interpreted as resulting from a relatively high velocity ($\sim$4700 km s^{-1}) 'bullet' of ^{56}Ni (Utrobin, Chugai & Andronova 1995). A similar geometry could potentially be applicable to SN 2011dh, assuming that a sizable (but slower) clump of ^{56}Ni was mixed into the oxygen layer. More sophisticated 3D nebular spectral modelling will be needed to constrain the geometry in more detail. For example, extending the secondary clump of our model by adding more material to the extreme redshifted edge (making the clump aspherical) would fill in the discrepancies apparent in the line profile near 6340 and 6420 Å, and would also more closely resemble the extended structures apparent in the models of Hammer et al. (2010, see their fig. 2).

Though the primary emitting sphere in our model is slightly offset from the origin, this may be due to uncertainty in the true SN Doppler velocity rather than an actual asymmetry of the ejecta. Though M51 is almost face-on, Tully (1974) shows that the southeast quadrant of M51 (where SN 2011dh occurred) is rotating towards us. The line-of-sight motion is significantly less than 250 km s^{-1} but the true Doppler velocity of M51 may be lower than the value we used to deredshift our spectra. Adopting $z = 0.00155 \pm 0.0002$ (Falco et al. 1999) instead of the $z = 0.002$ used in the rest of this paper places the primary emitting component at a blueshift of $\sim$120 km s^{-1}, within a factor of 2 of the expected line-of-sight rotational velocity of M51 at the SN position. In addition, there are narrow Hα lines from the host galaxy superimposed on our spectra (slight oversubtractions are apparent in both the 268 and 334 d spectra; see Fig. 2). Assuming that the strongest of these lines in our 268 d spectrum was emitted in the rest frame of the SN, we measure a Doppler velocity of $550 \pm 160\,\mathrm{km\,s^{-1}}$. Adopting this value places the primary component at a blueshift of $\sim$200 km s^{-1} relative to rest. It appears that the primary emitting component of SN 2011dh is either symmetric with respect to the rest frame or nearly so. Note, as well, that these relatively low Doppler velocities lie near the resolution limit of our spectra. As described by Silverman et al. (2012), our spectra have characteristic wavelength errors

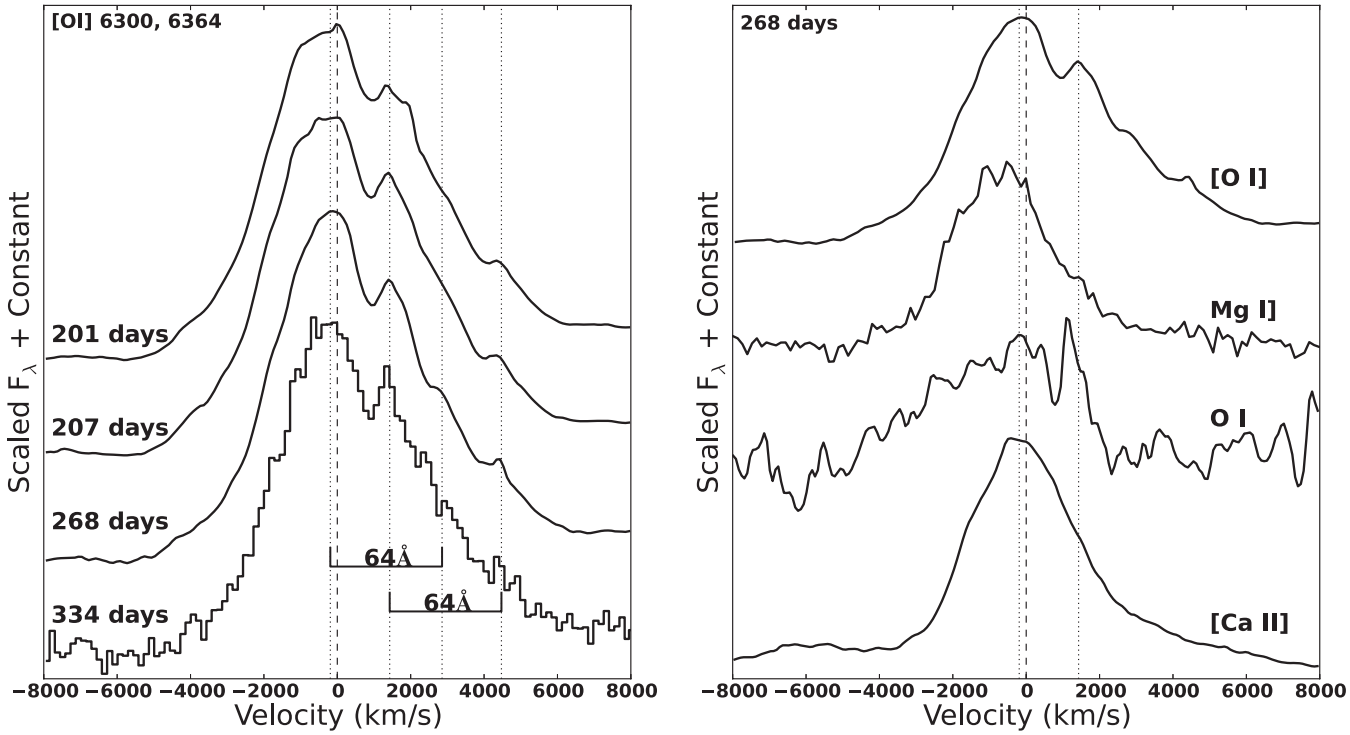

Figure 6. The [O I] λλ6300, 6364 doublet line profile during the early nebular phase of SN 2011dh (left) and the [O I] λλ6300, 6364, Mg I] λ4571, O I λ7774 and [Ca II] λλ7291, 7324 profiles of SN 2011dh 268 d after core collapse (right). The components described in Section 3.2 persist throughout the nebular phase with similar relative fluxes and wavelength offsets, and similar profiles are apparent in the [O I], Mg I] and O I lines. The vertical dotted lines show the best-fitting velocities of the two components of the [O I] λλ6300, 6364 line as described in Section 3.2 and shown in Fig. 5. The dashed line at 0 km s^{-1} marks the rest frame of M51.

of 1–2 Å ($\lesssim$90 km s^{-1}). The positions of most other nebular lines are consistent with this scenario (with widths of several thousand km s^{-1} and irregular profiles, it is difficult to determine the centres of nebular SN lines to high precision). The Mg I] λ4571 line is an exception, displaying a strong asymmetry and a blueshifted peak (see below).

As Fig. 6 shows, the components described above persist from 201 to 334 d, and similar components at similar relative positions are apparent in the O I λ7774 profile and the Mg I] λ4571 profile, though the primary component appears to be more blueshifted in Mg I]. The [Ca II] λλ7291, 7324 profile, however, exhibits a simple and singly peaked profile. Other studies have shown that it is common for Mg I] and [O I] to display similarly asymmetric line profiles while [Ca II] remains relatively symmetric (e.g. Modjaz et al. 2008; Milisavljevic et al. 2010).

SN 2011dh's nebular [O I] profile is not consistent with the often-proposed simple torus model of emitting material. An emission trough due to an overall torus-like geometry of emitting material would fall at the rest wavelength of the line (in the SN rest frame). As Fig. 5 shows, SN 2011dh instead displays an emission peak at roughly the rest wavelength; if the main trough in the line profile were associated with the centre of a torus, it would have to be offset from the rest frame of M51 by ∼1000 km s^{-1}, an offset inconsistent with the centres of other nebular emission lines. To explore this further we ran several models similar to the two-clump model described above but with a toroidal component at various viewing angles, and we found no physically plausible toroidal geometries that matched the profile well.

Maurer et al. (2010) showed that foreground Hα absorption was a reasonable explanation for the double [O I] peak in SN 2008ax. It is possible that foreground hydrogen absorption is also affecting the oxygen profile in SN 2011dh: early time spectra indicate a hydrogen expansion velocity of 12 500–15 400 km s^{-1} (velocities at 14 and 4 d; Marion et al. 2013), and the peak of [O I] emission is ∼12 000 km s^{-1} (265 Å) blueward of Hα. However, explaining all three bumps in the profile through foreground absorption would require three well-placed hydrogen overdensities, at ∼8100, 9600 and 11 100 km s^{-1}, and would not account for the line profiles of Mg I] λ4571 and O I λ7774. It seems apparent that the [O I] line-profile asymmetries in SN 2011dh come from distinct emitting components moving relative to each other, each displaying the doublet nature of the line. Additionally, the lack of obvious Hα absorption features may indicate a very low hydrogen shell mass.

4 NEBULAR MODELS

We use a spherically symmetric single-zone non-local thermodynamic equilibrium (LTE) nebular modelling code to further explore SN 2011dh. The code tracks the heating of the nebular ejecta through deposition of γ-rays and positrons produced by radioactive decay. This heating is balanced by line emission to determine both the temperature and ionization state of the nebula. Following methods and ideas first outlined by Axelrod (1980) and Ruiz-Lapuente & Lucy (1992), the code was developed by Mazzali et al. (2001), and has been described in greater detail by, for example, Mazzali et al. (2010) and Mazzali & Hachinger (2012).

The code is available in a one-zone version, a stratified version and a 3D version. The one-zone model provides a rough estimate of the properties of an SN nebular spectrum (e.g. mass and elemental abundances). The stratified model is preferred when comparing

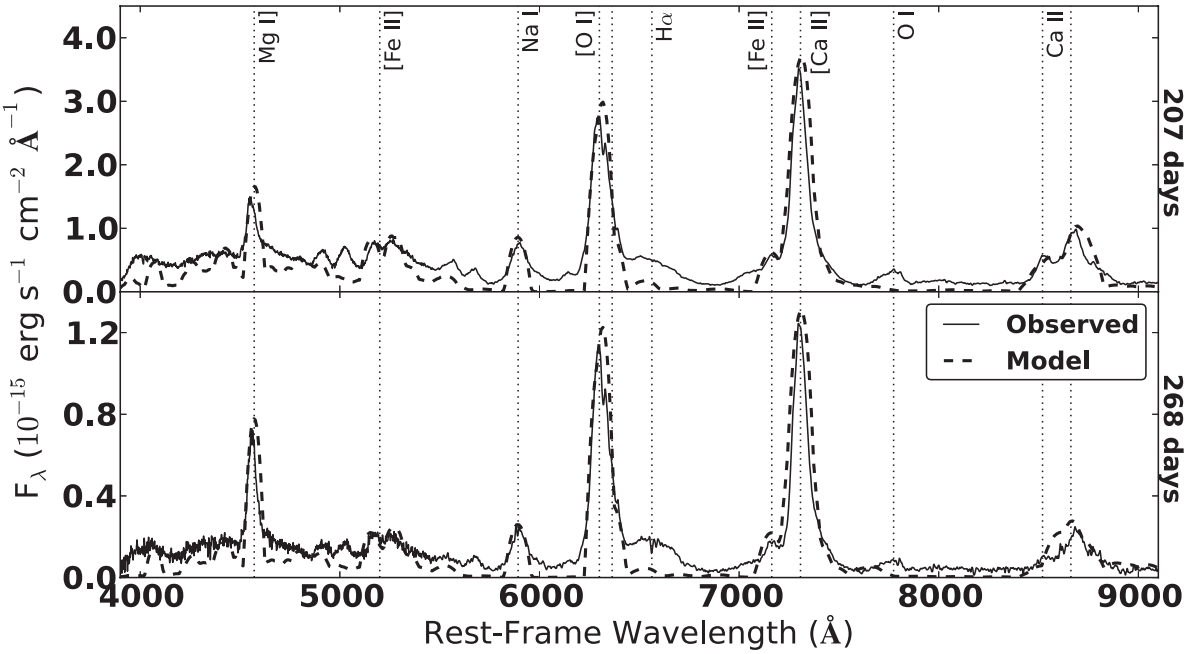

Figure 7. Comparison between our best-fitting nebular models and the observed spectra of SN 2011dh at 207 and 268 d after core collapse. See Section 4 for details.

a detailed model of the explosion with the data (Mazzali et al. 2007), and the 3D model is useful for strongly asymmetric events (Mazzali et al. 2005). Here, since the profiles of the emission lines do not deviate significantly from the theoretically expected parabolic profiles and developing a complete explosion model is beyond the scope of this paper, we restrict ourselves to the one-zone approach. Mass-estimate differences between the one-zone and the stratified model are relatively small in cases where the ejecta do not display strong asphericity (∼20 per cent; Mazzali et al. 2001). The code does not include recombination emission, and therefore neither Hα nor the O I λ7774 recombination lines are reproduced. While hydrogen is located outside the carbon–oxygen core and ignoring Hα does not affect our result, ignoring the oxygen recombination line can introduce an error, though it should be small (Maurer et al. 2010). Another element of uncertainty is introduced by the fact that silicon does not have strong lines in the optical range. The strongest line, [Si I] λ6527, is about one third as strong as Na I D and is swamped by the Hα emission. All these effects could lead to an overestimate of the mass. Finally, a major source of uncertainty is the subtraction of the background pseudo-continuum.

Our best-fitting models to the day 207 and 268 spectra are shown in Fig. 7. The spectrum of SN 2011dh changes only slightly between these two epochs, and the two (independent) models are very similar. These models are powered by ∼0.07 $M_\odot$ of ^{56}Ni and exhibit an outer envelope velocity of ∼3500 km s^{-1} with a total enclosed mass of ∼0.75 $M_\odot$. See Table 4 for a detailed listing of the mass composition of the models. Note that these values are sensitive to errors in the determination of the distance to SN 2011dh and errors in the absolute flux calibration of our spectra. Most of the major features of these spectra are matched by the models, including the prominent [Ca II] λλ7291, 7324, [O I] λλ6300, 6364, Na I D and Mg I] λ4571 lines.

Bersten et al. (2012) derived a similar but slightly lower ^{56}Ni mass of ∼0.065 $M_\odot$ from bolometric light-curve modelling through the first 80 d, while Sahu et al. (2013) derived a slightly higher mass of ∼0.09 $M_\odot$ through an analytic treatment of the bolometric light-curve peak. Several other SNe IIb have been modelled in their nebular phase with similar codes, providing a useful set for comparison. Our models of SN 2011dh include ∼0.26 $M_\odot$ of oxygen, much less than that was needed for SNe 2008ax, 2001ig and 2003bg (∼0.51, 0.81 and 1.3 $M_\odot$, respectively; Mazzali et al. 2009; Silverman et al. 2009; Maurer et al. 2010). The ^{56}Ni mass required is also relatively low. SN 2011dh had ∼0.067 $M_\odot$ of nickel, but as the above authors have shown, SNe 2008ax, 2001ig and 2003bg required ∼0.10, 0.13 and 0.17 $M_\odot$, respectively. This indicates a relatively low-mass progenitor for SN 2011dh.

On the other hand, it is unclear whether the nebular spectra capture all of the carbon–oxygen core. The lowest velocity of the He lines is ∼5000 km s^{-1}, while the width of the emission lines is only ∼3500 km s^{-1}. Material between these two velocities may not be captured by the nebular modelling. Although this would go in the direction of compensating for the overestimate described above, we conservatively assign an error of ∼±50 per cent in our mass estimates. It would be interesting to test the data against realistic explosion models in order to narrow down this uncertainty. This will be the subject of future work.

Table 4. Nebular model mass composition.

Element	Mass ($M_\odot$) day 207	Mass ($M_\odot$) day 268
C	7.0×10^{-2}	6.0×10^{-2}
O	2.6×10^{-1}	2.8×10^{-1}
Na	1.3×10^{-4}	1.7×10^{-4}
Mg	1.6×10^{-3}	4.2×10^{-3}
Si	3.0×10^{-1}	3.0×10^{-1}
S	2.3×10^{-2}	2.5×10^{-2}
Ca	9.1×10^{-3}	1.0×10^{-2}
Fe	1.0×10^{-2}	1.0×10^{-2}
^{56}Ni	6.7×10^{-2}	7.0×10^{-2}
Total	7.4×10^{-1}	7.6×10^{-1}

Note. Mass composition of non-LTE nebular models fit to spectra of SN 2011dh at 207 and 268 d after core collapse.

Multiple groups have modelled the nucleosynthetic yields of core-collapse SNe of various zero-age main-sequence masses (e.g. Woosley, Langer & Weaver 1995; Thielemann, Nomoto & Hashimoto 1996; Nomoto et al. 2006). Though there are some discrepancies between our nebular model and the nucleosynthetic models (and some disagreements between different nucleosynthetic modelling efforts), our models are most consistent with a progenitor mass of 13–15 $M_\odot$. For example, Thielemann et al. (1996) predict carbon yields of 0.06, 0.08 and 0.115 $M_\odot$ and oxygen yields of 0.218, 0.433 and 1.48 $M_\odot$ for 13, 15 and 20 $M_\odot$ progenitors, respectively. The values required by our best-fitting model, 0.07 $M_\odot$ of carbon and 0.26 $M_\odot$ of oxygen, indicate a 13–15 $M_\odot$ progenitor. Note that not all elements are in such good agreement.

This result corroborates the findings of several other groups: the progenitor of SN 2011dh was a relatively low-mass ($\sim$13–17 $M_\odot$) YSG that likely had its outer envelope stripped away by a binary companion (e.g. Maund et al. 2011; Murphy et al. 2011; Benvenuto et al. 2012; Bersten et al. 2012; Van Dyk et al. 2013). SN 2011dh has provided a powerful test of the accuracy of SN progenitor studies through nebular spectra. The clear agreement between the nebular modelling and the results of such varied studies indicates that models of nebular SN spectra provide real and powerful constraints of the progenitor's properties. There is, however, work to be done to understand the discrepancies between modelled nucleosynthetic yields and nebular spectra models.

5 CONCLUSIONS

SN 2011dh was a very nearby SN IIb discovered in M51 in early 2011 June, providing observers with a valuable opportunity to track the evolution of one of these relatively rare SNe in detail. The nature of SN 2011dh's progenitor star has been much debated. In this paper, we present nebular spectra from 201 to 678 d after explosion as well as new modelling results. We confirm that the progenitor of SN 2011dh was a star with a zero-age main-sequence mass of 13–15 $M_\odot$, in agreement with the photometric identification of a candidate YSG progenitor.

In addition, our spectra at $\sim$2 yr show that photometric observations taken near that time are dominated by the fading SN and not, for example, by a background source or a binary companion. We present evidence pointing towards interaction between the expanding SN blast wave and a circumstellar medium, and show that the SN enters the positron-dominated phase by $\sim$1 yr after explosion. Finally, we explore the geometry of the ejecta through the nebular line profiles at day 268, concluding that the ejecta are well fitted by a globally spherical model with dense aspherical components or clumps. In addition to the data presented here we have obtained several epochs of spectropolarimetry of SN 2011dh as it evolved. The analysis of those data is beyond the scope of this paper, but they will provide additional constraints on any asymmetry in the explosion of SN 2011dh.

ACKNOWLEDGEMENTS

Sincere thanks to all of the supernova experts who contributed through discussions, including (but not limited to) Brad Tucker, WeiKang Zheng, Ori Fox, Patrick Kelly and J. Craig Wheeler (whose keen eye identified a significant typo in the manuscript). We thank the referee for suggestions that helped to improve this paper. Some of the data presented herein were obtained at the W. M. Keck Observatory, which is operated as a scientific partnership among the California Institute of Technology, the University of California and the National Aeronautics and Space Administration (NASA); the observatory was made possible by the generous financial support of the W. M. Keck Foundation. The authors wish to recognize and acknowledge the very significant cultural role and reverence that the summit of Mauna Kea has always had within the indigenous Hawaiian community; we are most fortunate to have the opportunity to conduct observations from this mountain.

This material is partially based upon work supported by a National Science Foundation (NSF) Graduate Research Fellowship to JB under grant no. DGE 1106400. JMS is supported by an NSF Astronomy and Astrophysics Postdoctoral Fellowship under award AST-1302771. AVF and his SN group at UC Berkeley acknowledge generous support from Gary and Cynthia Bengier, the Richard and Rhoda Goldman Fund, the Christopher R. Redlich Fund, the TABASGO Foundation and NSF grant AST-1211916. This research has made use of NASA's Astrophysics Data System Bibliographic Services, as well as the NASA/IPAC Extragalactic Database (NED) which is operated by the Jet Propulsion Laboratory, California Institute of Technology, under contract with NASA.

REFERENCES

Arcavi I. et al., 2011, ApJ, 742, L18
Arnett D., 1996, Supernovae and Nucleosynthesis: An Investigation of the History of Matter, from the Big Bang to the Present. Princeton Univ. Press, Princeton
Axelrod T. S., 1980, PhD thesis, Univ. California
Benvenuto O. G., Bersten M. C., Nomoto K., 2012, ApJ, 762, 74
Bersten M. C. et al., 2012, ApJ, 757, 31
Bietenholz M. F., Brunthaler A., Soderberg A. M., Krauss M., Zauderer B., Bartel N., Chomiuk L., Rupen M. P., 2012, ApJ, 751, 125
Campana S., Immler S., 2012, MNRAS, 427, L70
Cardelli J. A., Clayton G. C., Mathis J. S., 1989, ApJ, 345, 245
Chevalier R. A., Fransson C., 1994, ApJ, 420, 268
Chornock R. et al., 2011, ApJ, 739, 41
Chugai N. N., 1992, SvA, 18, L239
Colgate S. A., McKee C., 1969, ApJ, 157, 623
Ergon M. et al., 2013, preprint (arXiv:1305.1851)
Faber S. M. et al., 2003, Proc. SPIE, 4841, 1657
Falco E. E. et al., 1999, PASP, 111, 438
Feldmeier J. J., Ciardullo R., Jacoby G. H., 1997, ApJ, 479, 231
Filippenko A. V., 1982, PASP, 94, 715
Filippenko A. V., 1988, AJ, 96, 1941
Filippenko A. V., 1997, ApJ, 35, 309
Filippenko A. V., Sargent W. L. W., 1989, ApJ, 345, L43
Filippenko A. V., Matheson T., Ho L. C., 1993, ApJ, 415, L103
Filippenko A. V., Matheson T., Barth A. J., 1994, ApJ, 108, 2220
Fox O. D., Filippenko A. V., Skrutskie M. F., Silverman J. M., Ganeshalingam M., Cenko S. B., Clubb K. I., 2013, AJ, 146, 2
Fransson C., 1984, A&A, 133, 264
Fransson C., Chevalier R. A., 1989, ApJ, 343, 323
Griga T. et al., 2011, CBET, 2736, 1
Hammer N. J., Janka H.-T., Müller E., 2010, ApJ, 714, 1371
Hamuy M. et al., 2009, ApJ, 703, 1612
Hanuschik R. W., Thimm G., Dachs J., 1988, MNRAS, 234, 41p
Horesh A. et al., 2012, MNRAS, preprint (arXiv:1209.1102)
Houck J. C., Fransson C., 1996, ApJ, 456, 811
Jeffery D. J., Branch D., 1990, in Wheeler J. C., Piran T., Weinberg S., eds, Jerusalem Winter School for Theoretical Physics, Supernovae. World Scientific Press, Singapore, p. 149
Jerkstrand A., Fransson C., Maguire K., Smartt S., Ergon M., Spyromilio J., 2012, A&A, 546, A28

Krauss M. I. et al., 2012, ApJ, 750, L40
Laidler V. G., Greenfield P., Busko I., Jedrzejewski R., 2008, in Varoquaux G., Vaught T., Millman J., eds, Proc. 7th Python in Science Conference (SciPy 2008). Pysynphot: A Python Re-Implementation of a Legacy App in Astronomy. Pasadena, CA, p. 36, available at: http://conference.scipy.org/proceedings/scipy2008/SciPy2008_proceedings.pdf
Law N. M. et al., 2009, PASP, 121, 1395
Li W., Filippenko A. V., 2011, Astron. Telegram, 3399, 1
Li H., McCray R., 1992, ApJ, 387, 309
Li W. et al., 2011, MNRAS, 412, 1441
Maeda K. et al., 2008, Science, 319, 1220
Marion G. H. et al., 2013, ApJ, preprint (arXiv:1303.5482)
Matheson T. et al., 2000a, AJ, 120, 1487
Matheson T., Filippenko A. V., Ho L. C., Barth A. J., Leonard D. C., 2000b, ApJ, 120, 1499
Maund J. R., Smartt S. J., Kudritzki R. P., Podsiadlowski P., Gilmore G. F., 2004, Nature, 427, 129
Maund J. R. et al., 2011, ApJ, 739, L37
Maurer I., Mazzali P. A., Taubenberger S., Hachinger S., 2010, MNRAS, 409, 1441
Mazzali P. A., Hachinger S., 2012, MNRAS, 424, 2926
Mazzali P. A., Nomoto K., Patat F., Maeda K., 2001, ApJ, 559, 1047
Mazzali P. A. et al., 2005, Science, 308, 1284
Mazzali P. A. et al., 2007, ApJ, 670, 592
Mazzali P. A., Deng J., Hamuy M., Nomoto K., 2009, ApJ, 703, 1624
Mazzali P. A., Maurer I., Valenti S., Kotak R., Hunter D., 2010, MNRAS, 408, 87
Milisavljevic D., Fesen R. A., Gerardy C. L., Kirshner R. P., Challis P., 2010, ApJ, 709, 1343
Miller J., Stone R., 1993, Lick Observatory Technical Report No. 66. Univ. California, Santa Cruz
Modjaz M., Kirshner R. P., Blondin S., Challis P., Matheson T., 2008, ApJ, 687, L9
Murphy J. W., Jennings Z. G., Williams B., Dalcanton J. J., Dolphin A. E., 2011, ApJ, 742, L4
Nomoto K., Tominaga N., Umeda H., Kobayashi C., Maeda K., 2006, Nucl. Phys. A, 777, 424
Oke J. B. et al., 1995, PASP, 107, 375
Patat F., Chugai N., Mazzali P. A., 1995, A&A, 299, 715
Rabinak I., Waxman E., 2011, ApJ, 728, 63
Rau A. et al., 2009, PASP, 121, 1334
Ruiz-Lapuente P., Lucy L. B., 1992, ApJ, 400, 127
Rush B., Malkan M. A., Edelson R. A., 1996, ApJ, 473, 130
Sahu D. K., Anupama G. C., Chakradhari N. K., 2013, MNRAS, 433, 2
Sasaki M., Ducci L., 2012, A&A, 546, A80
Schlegel D. J., Finkbeiner D. P., Davis M., 1998, ApJ, 500, 525
Silverman J. M., Mazzali P., Chornock R., Filippenko A. V., Clocchiatti A., Phillips M. M., Ganeshalingam M., Foley R. J., 2009, PASP, 121, 689
Silverman J. M., Filippenko A. V., Cenko S. B., 2011, Astron. Telegram, 3398, 1
Silverman J. M. et al., 2012, MNRAS, 425, 1789
Soderberg A. M. et al., 2012, ApJ, 752, 78
Stritzinger M. et al., 2009, ApJ, 696, 713
Suntzeff N. B., Phillips M. M., Elias J. H., Walker A. R., Depoy D. L., 1992, ApJ, 384, L33
Taubenberger S. et al., 2009, MNRAS, 397, 677
Taubenberger S. et al., 2011, MNRAS, 413, 2140
Thielemann F.-K., Nomoto K., Hashimoto M.-A., 1996, ApJ, 460, 408
Tonry J. L., Dressler A., Blakeslee J. P., Ajhar E. A., Fletcher A. B., Luppino G. A., Metzger M. R., Moore C. B., 2001, ApJ, 546, 681
Tsvetkov D. Y., Volkov I. M., Sorokina E., Blinnikov S., Pavlyuk N., Borisov G., 2012, Perem. Zvezdy, 32, 6
Tully R. B., 1974, ApJS, 27, 437
Tully R. B., Fisher J. R., 1988, Catalog of Nearby Galaxies, Cambridge Univ. Press, Cambridge
Utrobin V. P., Chugai N. N., Andronova A. A., 1995, A&A, 295, 129
Van Dyk S. D. et al., 2011, ApJ, 741, L28
Van Dyk S. D. et al., 2013, ApJ, 772, L32
Vinkó J. et al., 2012, A&A, 540, A93
Woosley S. E., Pinto P. A., Martin P. G., Weaver T. A., 1987, ApJ, 318, 664
Woosley S. E., Langer N., Weaver T. A., 1995, ApJ, 448, 315
Yaron O., Gal-Yam A., 2012, PASP, 124, 668

This paper has been typeset from a TEX/LATEX file prepared by the author.